Organic Electronics 37 (2016) 386–395

Contents lists available at ScienceDirect

Organic Electronics

journal homepage: www.elsevier.com/locate/orgel

Degradation by ultra-violet light and its mechanism in organic solar cells

Hiroaki Sato, Wafa Syakira Binti Azmi, Yukio Onaru, Kenji Harafuji*

Department of Electrical and Electronic Engineering, Ritsumeikan University, Kusatsu, Shiga 525-8577, Japan

ARTICLE INFO

Article history:
Received 23 March 2016
Received in revised form
5 July 2016
Accepted 9 July 2016
Available online 22 July 2016

Keywords:
Organic solar cells
Illumination stress
Long-pass filter
Device degradation
UV light

ABSTRACT

We experimentally investigate the optimum illumination wavelength range and the degradation mechanism by the ultra-violet (UV) light for small-molecule organic solar cells (OSCs) using various long-pass filters with different cutoff wavelengths λ_c. The OSC structure consists of an indium–tin–oxide (ITO, anode)/copper phthalocyanine (CuPc, donor)/fullerene (acceptor)/bathocuproine (buffer)/Ag (cathode). The initial power conversion efficiency η_p is not affected by the use of the long-pass filter with $\lambda_c < 400$ nm. As λ_c increases above 400 nm, the initial η_p decreases significantly accompanied by a significant decrease in the short-circuit current, since the total amount of light energy absorbed in the OSC is decreased. The degradation of the OSC is investigated by repeating 30 s cycles, each consisting of 3 s of illumination followed by 27 s in the dark. The curve of the current J_L vs voltage V under illumination becomes strongly S-shaped at the 100th illumination cycle for $\lambda_c < 400$ nm, showing degradation. In contrast, for $\lambda_c > 400$ nm, no distinct degradation appears. Thus, the origin of the degradation is revealed to be UV light with wavelengths less than 400 nm. The degradation mechanism is attributed to the decrease in carrier transport efficiency at the interface between ITO and CuPc film. Reorganization of the CuPc crystal structure occurs in the near-surface region on ITO due probably to the heat generated by the UV light. This would deteriorate the electrical contact at the interface, resulting in an increase in series resistance there.

1. Introduction

Organic solar cells (OSCs) have attracted increasing interest as a promising alternative to inorganic solar cells because of their numerous desirable properties such as low-cost fabrication, flexible structure, and large-area application. The first major breakthrough in OSCs came in 1986 when Tang introduced the concept of the donor–acceptor (D/A) heterojunction based on small molecular materials fabricated by vacuum deposition [1]. The power conversion efficiency η_p of OSCs has steadily improved through the use of new materials [2–4], cathode buffer layers [5–7], and codeposited interlayer of donor and acceptor materials [8,9]. The lifetime of OSCs without any encapsulation, however, is still too short (less than a day in the dark and in air).

To date, several degradation mechanisms have been reported, e.g., the diffusion of molecular oxygen, water, and metal atoms into the device; degradation of interfaces; degradation of the active material; interlayer and electrode diffusion; the reaction of the electrode with organic materials; and morphological changes [10]. These mechanisms may be driven by illumination, by exposure to ambient air, or by temperature. The effect of three types of stress, namely, repetitive illumination, exposure to air, and repetitive electrical stress, on the degradation of small-molecule OSCs has been studied systematically [11]. Both repetitive illumination and air exposure appreciably deteriorate the device performance. The decrease in power conversion efficiency is dominated by a decrease in fill factor (*FF*). Of the several possible stresses, device degradation by illumination stress should receive special attention because OSCs generate power only when illuminated.

The degradation of OSCs is frequently accompanied by a degradation of the current–voltage (J–V) characteristics from an exponential diode curve to a curve with an S-shaped kink in the positive bias region [12–21]. This leads to decreases in both *FF* and η_p [22]. Several theoretical models proposed explanations for the mechanism behind the S-shaped kink in the J–V curve [19–23], e.g., corroded metal contacts and a thin current-limiting layer [20], charge accumulation induced by the cathode buffer layer [21], or

* Corresponding author.
E-mail address: harafuji@se.ritsumei.ac.jp (K. Harafuji).

http://dx.doi.org/10.1016/j.orgel.2016.07.011
1566-1199/

charge blocking due to the presence of strong interface dipoles [23].

In pentacene/fullerene (C_{60}) heterojunction OSCs, an experimental study under constant solar illumination indicated that two mechanisms were simultaneously responsible for degradation: photooxidation resulting in a drop in photocurrent and an ultraviolet (UV) annealing effect that reduces *FF* [12]. Differences in the temporal changes of the *J–V* characteristics appear clearly in devices that are kept in air, under vacuum, and under vacuum with a UV filter. In encapsulated polymer/C_{60} OSCs, thermal stress and visible light saturation have been shown to lead to severe degradation of the cells [24].

The S-shaped kink, however, has been overcome by the use of appropriate electrode and buffer materials, surface treatments, and doping [25]. Oida and Harafuji demonstrated that high resistance to the injection current at the organic/electrode interface is responsible for the S-shaped kink [22]. To suppress the kink, they proposed a device structure consisting of a set of thin Ag and pentacene layers between the anode electrode and the donor organic layer. Although there have been several phenomenological reports on the degradation of OSCs by illumination, the mechanism remains not well understood.

In this work, we experimentally investigate the effect of illumination stress on both the initial performance and the degradation phenomena of small molecule OSCs. We particularly consider the wavelength range of the illuminating light, which is controlled by a long-pass filter. Device parameters are monitored as a function of the number of repeated illuminations. UV light with wavelength less than 400 nm is shown to be responsible for device degradation. Preliminary results of this work have been reported elsewhere [26].

2. Experimental methods

Fig. 1(a) shows schematically the structure of the OSC investigated in this work. The OSC consists of an indium–tin–oxide (ITO) as the anode, a 20-nm-thick copper phthalocyanine (CuPc) layer as the donor, a 40-nm-thick C_{60} layer (SES Research, 99.9%) as the acceptor, a 10-nm-thick bathocuproine (BCP) layer (Tokyo Kasei, refined product) as the cathode buffer layer, and a Ag layer as the cathode. The CuPc (Aldrich, 90%) is purified three times by thermal gradient sublimation before use. The other organic materials are used as received.

Fig. 1(b) shows schematically the structure of the hole-only device. The simple structure reduces the number of unnecessary interfaces in the OSC [27], allowing us to focus on the changes in the bulk layer of CuPc and at the ITO/CuPc interface. A compound electrode composed of a 20-nm-thick Au layer and 80-nm-thick Ag layer is used as the cathode. Here, CuPc is in direct contact with Au on the cathode side. The work function of ITO is 4.7 eV and that of Au is 5.1 eV. The highest occupied molecular orbital of CuPc is 5.2 eV. Thus, a high barrier to hole injection exists at the ITO/CuPc interface, whereas the barrier at the Au/CuPc interface is small.

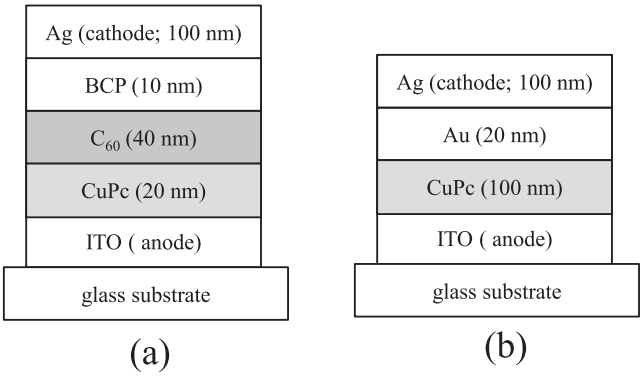

Fig. 1. (a) Schematic of the structure of the organic solar cell investigated in this work. (b) Schematic of the structure of the hole-only device.

Six devices are fabricated on ITO-precoated glass substrates (Mitsuru Optical Laboratory) with the size of 2.0 cm × 2.5 cm. The thickness of the ITO is 1450 ± 100 Å, the sheet resistance is less than 15 Ω/square, and the root-mean-square of the ITO surface roughness is 2.54 nm [28]. The ITO substrate is cleaned three times through ultrasonic treatment in detergent, deionized water, acetone, and then ethanol, in that order, for 5 min each. No further treatment of the ITO (e.g., UV ozone treatment) is done. Organic materials are evaporated on the ITO substrate at a rate of 0.5 Å/s under a pressure of less than 1.0×10^{-3} Pa (ULVAC KIKO VFR-200M/ERH). The deposition rate is monitored using an oscillation quartz microbalance (ULVAC CRTM-6000). The Ag top electrode is thermally evaporated through a stainless-steel mask with a 6 mm^2 active area of 2.4×2.5 mm^2.

The device is illuminated through the ITO bottom electrode. The *J–V* curves are measured using an electrometer (ADC 6241A) and an electric automatic shutter (Agilent 34970A/34903A). The device is illuminated by a 100 mW/cm^2 Xenon lamp, and an air mass 1.5 global (AM1.5G) spectrum is obtained using a solar simulator (SAN-EI Electric XES-40S1). The intensity of the simulator output is calibrated using crystalline silicon solar cells with a 320–1100 nm broadband response (Axis Net ANS-002A). Data acquisition software (Sunrise W32-R6244S0L3-R) is used to evaluate the *J–V* characteristics.

A small stainless steel chamber with a glass illumination window is used to measure the device performance with the device under high vacuum. Fig. 2 shows photographs of the chamber. Fig. 2(a) shows a detailed view, where a mounted OSC can be seen through the glass illumination window. Here, a long-pass filter with cutoff wavelength λ_c is set on the glass illumination window. The filter only transmits light with wavelength longer than λ_c into the OSC. Six types of filter with $\lambda_c = 0$, 320, 370, 400, 550, and 665 nm are used. Here, $\lambda_c = 0$ nm corresponds to the case without the long-pass filter. Fig. 2(b) shows an overall view in which electrical wires and an evacuation port can be seen. Evacuation is done using a rotary pump.

A foreline trap (ULVAC OFI-050C) is installed between the chamber and the rotary pump to reduce the influence of oil mist from the rotary pump on the device. The pressure between the chamber and the foreline trap is approximately 7.0 Pa. The transmittance of the glass illumination window is 92% for visible and infrared light with wavelengths less than 2000 nm. However, the transmittance for UV light is 90%–92% for wavelengths between 300 and 400 nm, 84% at 250 nm, and 36% at 200 nm. No correction is made in the *J–V* measurements to compensate for the attenuation of light intensity by the glass illumination window.

Fig. 3 shows the experimental procedure used to investigate how the illumination wavelength (using the long-pass filter) affects device performance. The experiment is composed of two cases: Case I measures the *J–V* characteristics without the long-pass filter, and Case II measures the *J–V* characteristics with the long-pass filter. Here, Case I and Case II experiments are conducted separately. In other words, the device in Case I is different from that in Case II. Devices are installed in the small stainless steel chamber immediately after they are fabricated.

The experimental procedure is composed of four steps. All experiments are done under high-vacuum conditions. Step 1 is device selection, which is done before the degradation measurement. Generally, some devices on ITO substrates operate properly, but other devices operate poorly because of faulty device fabrication. To identify the device with the best performance, J_D–*V* measurements